Journal of Ocean Engineering and Marine Energy (2024) 10:489–507
https://doi.org/10.1007/s40722-024-00324-2

RESEARCH

Variations in wind wave parameters measured in the coastal waters of north-eastern Bay of Bengal

T. M. Anju[1] · V. Sanil Kumar[1,2] · Rabindro Nath Samal[3]

Received: 18 August 2023 / Accepted: 20 March 2024 / Published online: 30 April 2024

Abstract
Characteristics of the wind waves measured in the coastal waters of the northeastern Bay of Bengal are examined for 4 years. A comparison of the energy wave period (T_e) with different wave periods shows that the average wave period ($T_{m-1,1}$), significant wave period ($T_{1/3}$), and integral period (T_i) are closer to T_e. A maximum wave height of 5.5 m is observed, and the most typical values for the wave period range between 4 and 6.5 s. The steepness of the highest wave is 0.058. In the coastal waters, the values of the peak wave period (T_p) indicate a swell dominance in the monsoon. Short-period waves (T_p < 6 s) are relatively higher in 2015 and the long-period waves (T_p > 8 s) in 2013 and the changes are due to the variations in monsoon. A large number of long-period waves is observed during the northeast monsoon. Thirty-seven freak wave events occurred, and the presence of freak waves is higher in the monsoon. Interannual variations in the mean of T_{avg} are up to 5% and that of the 90-percentile of the average wavelength (λ_{Tavg}) is up to 10%. The annual mean wave power is 5 kW/m and annually during 25% of the time, the wave power is more than 7 kW/m.

Keywords Ocean sciences · Surface gravity waves · Wavelength · Wave spectral parameters · Wave steepness · Freak waves

List of symbols

H_s	Significant wave height, $4\sqrt{m_o}$
T_p	Peak wave period
T_{m01}	Mean period, m_0/m_1
T	Individual wave period
T_{m02}	Mean zero-crossing wave period, $\sqrt{\frac{m_0}{m_2}}$
$T_{m-1,1}$	Average wave period, $\sqrt{\frac{m_{-1}}{m_1}}$
T_{avg}	Average wave period in a record of 30-min
$T_e = T_{m-1,0}$	Wave energy period, $\frac{m_{-1}}{m_0}$
T_i	Integral period, $\sqrt{\frac{m_{-2}}{m_0}}$
$T_{H\max}$	Period of the highest wave
$T_{1/10}$	Average period of 10% highest waves
$T_{1/3}$	Significant wave period, average period of 33% highest waves
T_c	Crest period, mean time interval for the local maxima, sqrt (m_2/m_4)
T_{dw1}	Sqrt(m[– 1,2]/m_0)
$m_n = \int_0^\infty f^n S(f)\mathrm{d}f$, $n = 0,\ 1,\ 2,\ -1$	Where m_n is the nth order spectral moment and $S(f)$ is spectral energy density at frequency f
λ	Wavelength as per dispersion relationship from period
λ_X	Wavelength estimated from wave period X

✉ V. Sanil Kumar
sanil@nio.org

[1] Ocean Engineering Division, CSIR-National Institute of Oceanography (Council of Scientific & Industrial Research), Dona Paula, Goa 403 004, India

[2] Academy of Scientific and Innovative Research (AcSIR), Ghaziabad, Uttar Pradesh 201002, India

[3] Chilika Development Authority, Palaspalli, Pokhariput Road, Bhubaneswar, Odisha 751020, India

1 Introduction

The wave period and wavelength fluctuate based on the prevailing local and remote weather conditions. The wave period affects vessel stability and the safety of maritime operations. Longer-period waves tend to have smoother crests

and troughs, making navigation and ship operations more manageable. Short-period waves, on the other hand, can be choppier and more challenging to navigate, especially for smaller vessels. Hence, knowing the wave period helps ship captains, maritime authorities, and port operators make informed decisions regarding navigation, port operations, and the safety of vessels. Waves with longer lengths tend to have a deeper influence on nearshore processes, such as sediment transport and beach erosion, and coastal morphology. Since the wavelength is directly related to the energy carried by waves, understanding the wavelength also helps in predicting the impact of waves on coastal areas and designing appropriate coastal protection measures. Waves can have different combinations of wavelength and amplitude, leading to variations in energy.

The interaction between waves and structures depends on the relative size of the structure compared to the wavelength. Hence, in coastal engineering projects, such as the design of breakwaters, seawalls, and harbour structures, knowledge of wavelength is crucial. Depending on the application, the dominant wave period for a given sea state is defined by several approaches. The different wave periods estimated from zero crossing analysis and spectral analysis are used in various studies. Knowledge of the relationship between various wave periods helps coastal managers and researchers estimate the required wave period from the known values of other periods. Joint probability distribution of wave heights and wave periods is used for assessing the period for a given wave height (Longuet-Higgins 1983). The bivariate lognormal distribution proposed by Ochi (1978) is widely used to describe the joint characters of wave heights and periods (Zhao et al. 2022). Based on the long-term statistics of the waves in the China Sea and the Northwest Pacific Ocean, Fang and Hogben (1982) proposed a modified joint distribution model. Stansell et al. (2004) proposed a joint distribution function for waves in extreme storms and for moderately broad-banded spectra.

Higher wave steepness induces white capping and wave breaking in deep seas and is the primary sink of energy in the ocean (Perlin et al. 2013). Wave steepness increases in coastal seas since the wave height increases and wavelength decreases. When wave steepness enters the Stokes limit of 0.1428 tan$h$ (kd) (Stokes 1880), the wave becomes unstable and breaks at water depth (d). According to Mendes and Oliveira (2021), the steepness values of the most severe storms in the northeast Atlantic are higher than the yearly average. Steep waves contain more energy and are stronger, they can destroy the coastline faster and more severely than less steep waves (Kraus and Larson 1988). Hence, the steepness of waves can have a major impact on coastal erosion (Chen et al. 2023).

Bay of Bengal (BoB), a semi-closed tropical basin, is the largest bay in the world. The northwestern BoB, located in the northeastern part of the Indian Ocean, is influenced by the seasonal monsoon winds, with the southwest (SW) monsoon occurring from June to September and the northeast (NE) monsoon prevailing from October to December. These monsoons generate different wind patterns, which influence the waves. During the SW monsoon, strong winds from the southwest produce longer period waves, while the NE monsoon generates shorter period waves due to winds from the northeast. During the transition periods (May and October) between the southwest and northeast monsoons, the wind patterns are more variable. As a result, the wave characteristics during these months vary as well. Wave periods may extend slightly, and longer-period swell waves generated by distant storms or swells may propagate into the region, resulting in larger and more consistent waves. The coastal areas of BoB are prone to tropical cyclones, which are intense low-pressure systems characterized by strong winds and high waves. These cyclones cause waves with significant wave heights (H_s) up to 9 m in the BoB (Amrutha et al. 2014) and cause storm surges and coastal flooding. The occurrence of tropical cyclones in BoB has an annual bimodal structure, with high occurrences in May and October–November (Balaguru et al. 2014). In the northwestern BoB, particularly during the winter, swell waves originating from the Indian Ocean or the southern BoB propagate into the region. Shorter period waves typically result from local wind activity, while longer period waves are generated by distant storms.

Kumar et al. (2014) reported that the seasonal average value of H_s varied from 0.8 m in the NE monsoon season to 1.3 m in the SW monsoon along the northwestern BoB. Based on the data from 8 to 13 October 2013 during the TC Phailin, Amrutha et al. (2014) reported that at 50 m water depth in the northwestern BoB, a maximum wave height (H_{max}) of 13.5 m is measured. Patra et al. (2016), based on data for the years 1994, 2008–2009, and 2013–2014, observed that the waves of Gopalpur are predominantly from the south during the SW monsoon and south-southeast for the rest of the year. Patra and Bhaskaran (2017) analysed the wave climate in the head BoB using a combination of satellite altimeter data and numerical models and observed significant seasonal and interannual variations in the wave climate of the head BoB. Based on the wave measurements carried out from February 2013 to December 2015 and the ERA-Interim reanalysis wave data from 1979 to 2015, Anjali Nair et al. (2018) described the spectral wave characteristics off Gopalpur in northwestern BoB. Anjali Nair et al. (2018) observed two well-differentiated wave systems, one young sea from the east-southeast and another more developed swell from the south, leading to bimodality in the wave spectrum in the northwestern BoB. Along the Indian shelf seas, the annual mean wave power is minimal at sheltered regions of the east coast with an annual mean wave power of 2.0 kW/m and a

maximum of the northern west coast (13.7 kW/m) (Amrutha and Kumar 2022).

Freak waves are waves that are higher than that are predicted for a particular sea state (Bitner-Gregersen et al. 1998, Gramstad et al. 2018). The presence of freak waves can be a major cause of ship accidents and hence the data of freak waves has a prior importance. Many oceanographers have examined the probability and mechanism of freak wave occurrences, as well as highlighted significant environmental conditions that lead to freak wave creation, to limit the possibility of marine mishaps. Several theories are explained about the causes and development of freak waves in the open ocean. Glejin et al. (2014), analysed the existence of freak waves in the coastal region of Ratnagiri in the eastern Arabian Sea. A freak wave is identified when the maximum wave height ($H_{\max}$)-to-significant wave height (H_s) ratio exceeds 2–2.2 (Muller et al. 2005). According to various researchers, the mechanism of trapping a wave by an opposing current generates a freak wave (Lavrenov 1998; Shrira and Slunyaev 2014). Haver (2001) reported that the ratio of maximum wave height ($H_{\max}$) to significant wave height (H_s) that is most likely to be exceeded in 1 out of 100 situations is roughly 2.0. Amrutha and Kumar (2017) noted that the $H_{\max}/H_s$ ratio ranges from 1.50–1.62 for several areas in the nearshore waters of the eastern Arabian Sea during the SW monsoon.

The main goal of this article is to analyse the various wave periods, their associated wavelengths, and steepness during monsoon months in the northeastern Bay of Bengal and to analyse the characteristics of freak waves that occurred. The influence of tides and currents on waves is not considered in the present study. This paper is structured as follows: Sect. 2 describes about data and methods used in the study. Section 3 provides detailed analyses of wave period, wavelength, wave steepness, and freak waves. Section 4 discusses the results and Sect. 5 summarizes the findings.

2 Data and methods

The study is based on measured wave data collected with a 0.9 m diameter Datawell Directional Waverider Mk III buoy (Datawell 2009) at Gopalpur along the northeastern BoB from 1 January to 31 December 2015, as well as 1 June to 31 August 2013, 2017, and 2018. The wave data are measured by the authors under the project funded by the Earth System Science Organization, Ministry of Earth Sciences, Government of India through the Indian National Centre for Ocean Information Services, Hyderabad. Figure 1 provides the geographical location (latitude 19.2657° N, longitude 84.94834° E) of the buoy. At the location of the buoy, the water depth is 15 m. The buoy is fixed to the seafloor by a 15-m-long 35-mm-diameter rubber cord and a 25-m-long 16-mm-diameter polypropylene rope. The buoy data are sampled at a frequency of 3.84 Hz and logged at 1.28 Hz and for the period selected, there are no data gaps. According to Datawell (2009), heave is measured with a 3% accuracy and a 1 cm resolution. The zero up-crossing approach is used to calculate the wave height (H) and period (T) (Tucker 1991). In a 30-min record, the average periods of 10% and 33%, i.e., $T_{1/10}$ and $T_{1/3}$, are calculated and employed in the analysis. The maximum wave height ($H_{\max}$) and the corresponding period ($T_{H\max}$) are analysed in terms of a 30-min period. By dividing the duration of the record by the number of crests in the record, the crest period (T_c) is estimated. T_{avg} is the proportion of a record's length to its total number of zero-up crossings.

Spectral analysis helps in characterizing wave conditions, identifying wave components, and understanding the complex nature of wave systems. The fast Fourier transform calculates the wave spectrum of the surface elevation from the measured heave data every 30 min. The obtained wave spectrum has a resolution of 0.005 Hz between 0.025 Hz and 0.1 Hz, and then it is 0.01 Hz till 0.58 Hz (Datawell 2009). The wave parameters used in the study and derived from the wave spectra are significant wave height (H_s), energy wave period (T_e), wave period corresponding to the mean frequency of the spectrum (T_{m01}), integral wave period (T_i), mean zero-crossing period (T_{m02}), T_{dw2}, T_{dw1}, and average wave period ($T_{m-1,1}$). The spectral peak period (T_p) is the wave period corresponding to the maximum spectral energy density.

By following the wave dispersion relation, the wavelength (λ) corresponding to different wave periods is determined from the wave period and the sea depth. The occurrence percentage of wave period is calculated with 0.5 s bin (0–0.5, 0.5–1,…) and 5 m bin (0–5, 5–10,…) for its corresponding wavelength. The 99 percentiles for June–August are taken as an extreme value index and are computed for all the wave periods. The interannual variations of wave period and wavelength are estimated based on the 99, 90 percentiles and mean values from the available data at Gopalpur. The 99 and 90 percentile wave period and its corresponding wavelength are calculated from the available half-hourly time series data. Wave steepness is estimated as the ratio of the wave height to the corresponding wavelength.

The joint probability distribution of wave heights and wave periods is examined with the bivariate lognormal distribution proposed by Ochi (1978) and the Fang and Hogben model (1982). The criteria used to estimate the freak wave events are (i) ratio of $H_{\max}/H_{1/3} > = 2.1$ and (ii) ratio of $H_c/H_{1/3} > = 1.25$, where $H_{\max}$, $H_{1/3}$, and H_c are defined as maximum wave height, and significant wave height and crest height of waves. Wave power (P) per unit circular area of the sea surface is calculated from spectral data using the

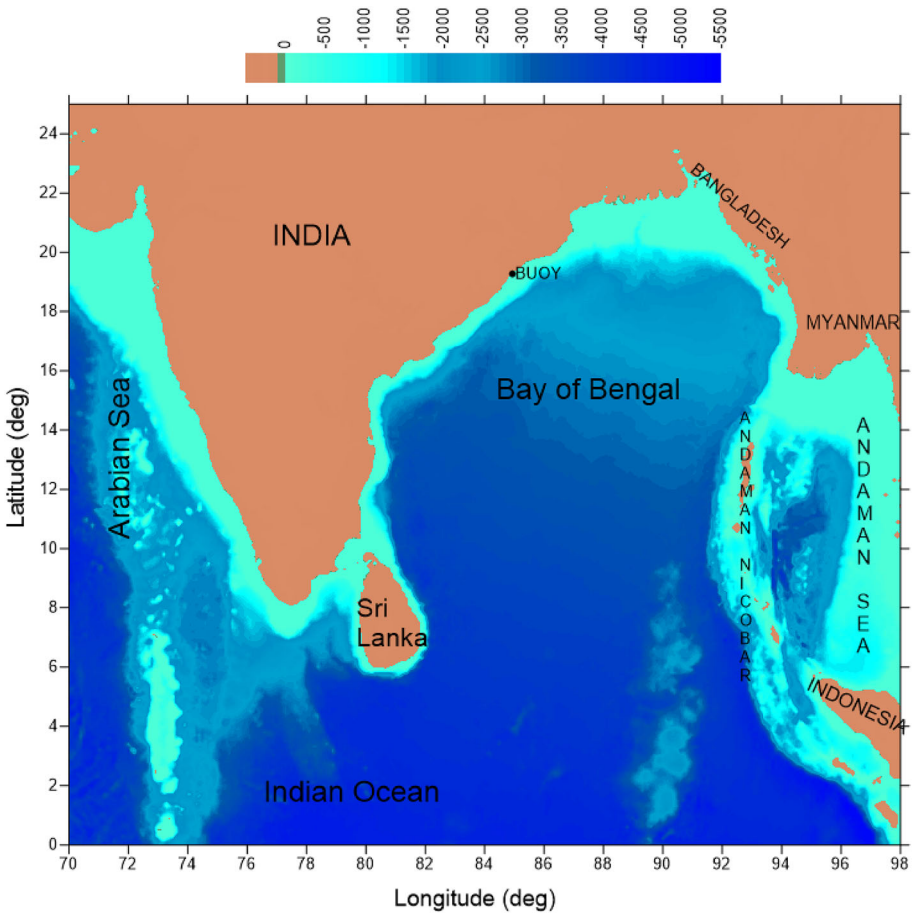

Fig. 1 Map showing the study area. Data used in the study are from the buoy located in the northeastern Bay of Bengal. The colour shade is the depth in metres

below expression:

$$P = \rho g \int_0^{2\pi} \int_0^{\infty} C_g(f, d) S(f, \theta) \mathrm{d}f \mathrm{d}\theta, \quad (1)$$

where ρ is seawater density (kg/m^3), d is the water depth (m), g is the gravitational acceleration (m/s^2), $S(f,\theta)$ is the directional wave spectral energy density (m^2/Hz/deg), θ is the wave direction (deg), and $C_g(f,d)$ is the wave group velocity (m/s) and is estimated using linear wave theory as given below (Coastal Engineering Manual 2008).

3 Results and discussion

3.1 Distribution of wave period

The probability of exceedance of the half-hourly average of various wave periods over different years from June to August is presented in Fig. 2. T_p provides information on the dominance of swells or wind-seas at a particular location. From hours to decades, waves exhibit fluctuations, and as a result, T_p also fluctuates. The annual average T_p for all the years in the study is up to 11.2 s. In most BoB locations, the average T_p is about 10–11 s during the peak monsoon months (June–August), when winds are significantly stronger (> 12 m/s) than in other months (George and Kumar 2021). The short-period waves (T < 6 s) are caused by wind-seas, long-period waves (T > 8 s) are dominated by swell and intermediate-period waves (6 s ≤ T ≤ 8 s) are caused by the swell (Bromirski et al. 2005). ~ 1% of T_p are less than 6 s and 86% are with values greater than 8 s, which indicates a swell dominance at Gopalpur from June to August. Swell dominant regions have a larger value for T_p and relatively low wind speed indicating an inverse relationship between those parameters.

In the coastal waters of Gopalpur, the 30-min mean values of the mean wave period range between 4 and 10.3 s (Fig. 2b), while 42% of T_{m02} values are shorter than 6 s. Statistical parameters of wave periods are listed in Table 1. The integral period (T_i) goes up to a maximum value of 15.9 s (Fig. 2c) with an annual average value of 9.5 s. Half of the records showed that the crest period (T_c) is shorter than 4 s in the northeastern BoB. A maximum value for the parameters T_p, and T_{Hmax} occurs in 2015 and 2018, and the other parameters reach a maximum value in the year 2013. T_{m01} is the parameter used to obtain the magnitude of Stokes drift

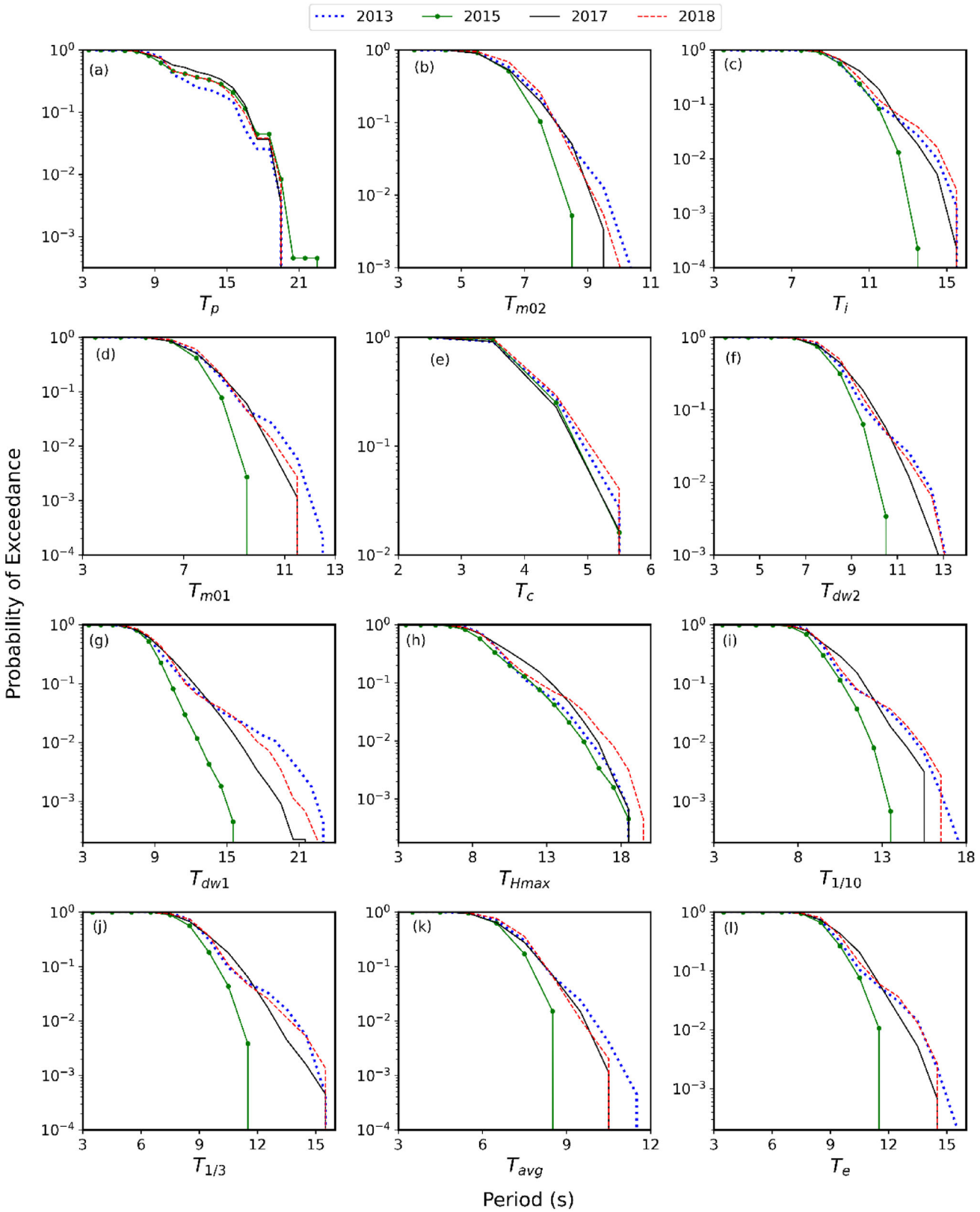

Fig. 2 Distribution of various wave periods at Gopalpur for 4 years during the monsoon months June to August

Table 1 Statistical parameters of different wave periods and corresponding wavelengths for the months June, July and August for different years (2013, 2015, 2017, and 2018)

Parameter	Minimum	Maximum	Mean	Mode	Standard deviation	90-percentile	99-percentile
Wave period (s)							
T_c	2.5	6.0	3.7	3.5	0.5	4.5	5.3
T_{m02}	4.0	10.3	6.3	5.9	0.9	7.4	8.7
T_{avg}	4.3	12	6.6	6.2	0.9	7.7	9.2
T_{m01}	4.5	12.2	7.1	6.8	1.0	8.3	10.1
T_e	5.6	15.1	8.8	7.9	1.2	10.3	12.8
T	1.6	23.8	6.5	5.3	2.8	10.2	14.5
$T_{1/3}$	5.2	15.6	8.6	8.5	1.2	10.1	12.8
T_i	6.4	15.9	9.5	8.7	1.3	11.2	13.8
T_{Hmax}	3.9	19.6	9.2	8.4	2.1	12.1	15.9
$T_{1/10}$	5.3	17.5	9.1	8.7	1.4	10.9	14.2
T_{dw1}	4.4	23.3	8.8	8.2	2.1	11.1	16.5
T_p	4.4	22.2	11.2	9.1	3.3	15.4	18.2
T_{dw2}	5.0	13.6	7.9	7.4	1.1	9.2	11.3
Wavelength corresponding to wave period (m)							
λ_{Tc}	9.4	53.0	21.8	19.0	6.5	31.0	42.0
λ_{Tm02}	25.4	112.6	56.7	50.8	13.1	73.7	91.8
λ_{Tavg}	28.8	135.3	61	55.9	13.2	77.5	98.2
λ_{Tm01}	32.0	138.4	68.9	64.0	14.3	86.3	110.9
λ_{Te}	46.9	174.6	92.2	87.2	16.3	112.5	145.2
λ_T	4.0	283.3	61.3	56.7	38.1	112	167.1
$\lambda_{T1/3}$	41.3	181.3	90.4	88.7	17.0	110.3	145.6
λ_{Ti}	58.8	185.1	102.7	92	17.1	125.2	158.7
λ_{THmax}	23.7	231.4	97.1	87.3	28.6	136.6	185.1
$\lambda_{T1/10}$	42.8	205.2	96.4	91.4	19.4	120.9	163.5
λ_{Tdw1}	30.5	277.6	92.1	85.1	28.1	123.9	192.5
λ_{Tp}	29.4	263.9	123.7	96.8	43.1	178.5	213.7
λ_{Tdw2}	39.0	155.6	80.0	73.0	14.9	98.0	126.2

(Stokes 1880) transport in the deep waters and the average value of T_{m01} is 7.1 s in the present study (Table 1). The maximum value of T_{m02} during non-monsoon months is up to 12.7 s, while during monsoon months, the value is about 8.5 s, showing a decrease in the values of T_{m02} during monsoon months. The 99-percentile values of T_{dw2} and T_{dw1} are 11.3 s and 16.5 s. Standard deviation values of T_{Hmax}, $T_{1/10}$, and $T_{1/3}$ are 2.1, 1.4, and 1.2 s (Table 1). When the spectral form is unknown, the energy wave period (T_e) can be calculated from other variables, such as the mean or peak period (Contestabile et al. 2015), since the values of T_e play a significant role in offshore power calculations. The mean values of T_{avg} and T_e are 6.6 and 8.8 s. The 90-percentile values of T_{Hmax}, T_{avg}, $T_{1/3}$, and T_e are 12.1, 7.7, 10.1, and 10.3 s (Table 1).

Figure 3a, b presents the percentage of occurrence of various wave periods during monsoon and non-monsoon months. In 2015, during the monsoon months, the percentage of $T_p < 6$ s was about 1.6%, while in non-monsoon months, the value is 9.3% and $T_p > 8$ s is around 81.3% in monsoon months and 88% in non-monsoon months. The percentage occurrence of T_c is 70.8% in between 3 and 4 s during monsoon (Fig. 3a), while 44% occurrence is seen during non-monsoon months (Fig. 3b). An occurrence of 40% is seen for $T_{1/10}$ and T_e, in between 8 and 9 s. During non-monsoon, the occurrence of $T_e > 12$ s is 6%, while there is no occurrence of $T_e > 12$ s during monsoon months. The significant wave period ($T_{1/3}$) plays a significant role in the design of coastal structures (Goda 2000) and the standard deviation of $T_{1/3}$ is 1.2 s.

3.2 Relationship between different wave periods

Scatter plots of different parameters with T_e are presented in Fig. 4a–h and the results indicate that only $T_{m-1,1}$, $T_{1/3}$

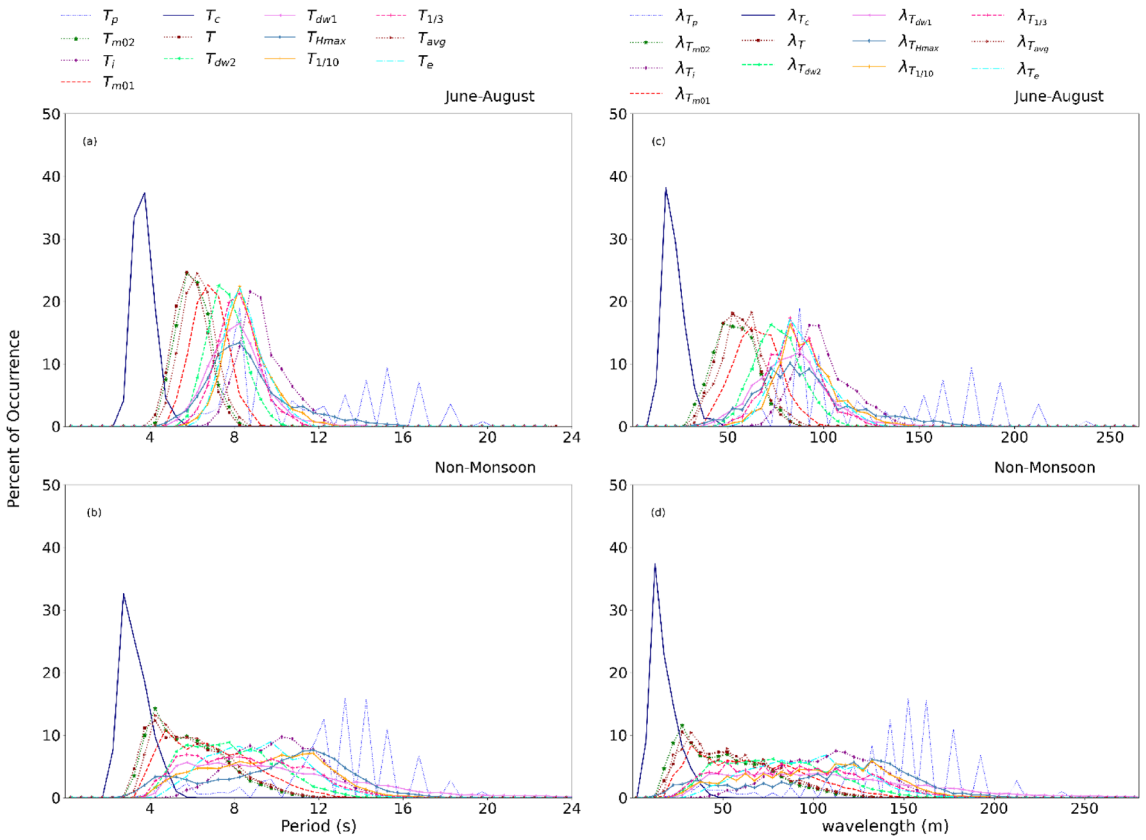

Fig. 3 Percentage occurrence of different wave period (**a**, **b**) and its corresponding wavelength (**c**, **d**) for monsoon months (June–August) and non-monsoon months for 2015

and T_i are almost close to the values of T_e. The scatter plot of T_e with T_p (Fig. 4e), T_{dw1} (Fig. 4f), and T_{Hmax} shows a wide scatter (Fig. 4g). $T_{1/3}$ and T_e are similar parameters (Goda 2000), and in the absence of T_e, T_p is used to compute the wave power (Contestabile et al. 2015). Since T_p values are significantly higher than T_e in the study area, computing wave power using T_p will result in a large overestimation of wave power. According to Hofland et al. (2017), several wave periods, including T_p and the primary zero-crossing period ($T_{1/3}$), are associated with a range of coastal activities for typical spectral shapes and deep-sea conditions.

The maximum wave height (H_{max}) in the coastal waters of Gopalpur is 5.5 m from June to August which is much less than the values observed during the tropical cyclone. The northern BoB at 21.00° N, 89.00° E experienced a greater H_{max} of ~ 17.9 m during the passage of tropical storm Aila (Kumar et al. 2020). The variation of H_s with H_{max} is presented in Fig. 4k and it shows H_{max} is 1.65 times H_s. The monthly average H_s varies from 1.37 to 1.73 m in different years. The scatter plot between T_{Hmax} and $T_{1/3}$ shows that T_{Hmax} has a wide range compared to $T_{1/3}$ (Fig. 4i), while $T_{1/3}$ is equal to 1.36 times T_{m02} (Fig. 4j). T_e estimates from T_p are lower ($T_e = 0.786\ T_p$) due to the presence of numerous wave systems, on comparison with the T_e estimates from the JONSWAP spectrum ($T_e = 0.9T_p$) and the Pierson—Moskowitz spectrum ($T_e = 0.86T_p$). The deep-water ratio of T_e/T_p ~ 0.9 for a single-peaked spectrum is frequently utilized in engineering to know the wave period near a structure's toe from a known offshore wave period T_p (Hofland et al. 2017). The slope value of T_e with T_i is close to 1, showing a linear relationship between both variables. Figure 4d indicates the relationship between T_e and $T_{1/3}$, T_e is about 1.03 times T_p, and both play a significant role in the design of coastal structures. During the cyclone Phailin (8–13 October 2013), waves off Gopalpur showed a mean wave period ranging from 6.6 to 8.6 s, and T_p ranging between 8.4 and 18.4 s (Amrutha et al. 2014). According to Chun and Ahn's (2017) model, with a maximum value of H_s around 5.35 m, the predicted and measured values for $T_{1/3}$ at Hamada during a storm period are 9.79 and 9.58 s. George and Kumar (2021) reported that the maximum monthly average T_p value over the BoB is 15 s and throughout the year in southeastern BoB, the occurrence of $T_p > 12$ s is larger. Despite the BoB being open to waves from the south IO and SO, significant longitudinal variation in T_p is seen. In the BoB, the values of T_p vary from a minimum of 2.7 s to a maximum of 21 s with an average value of 9.9 s (George and Kumar 2021).

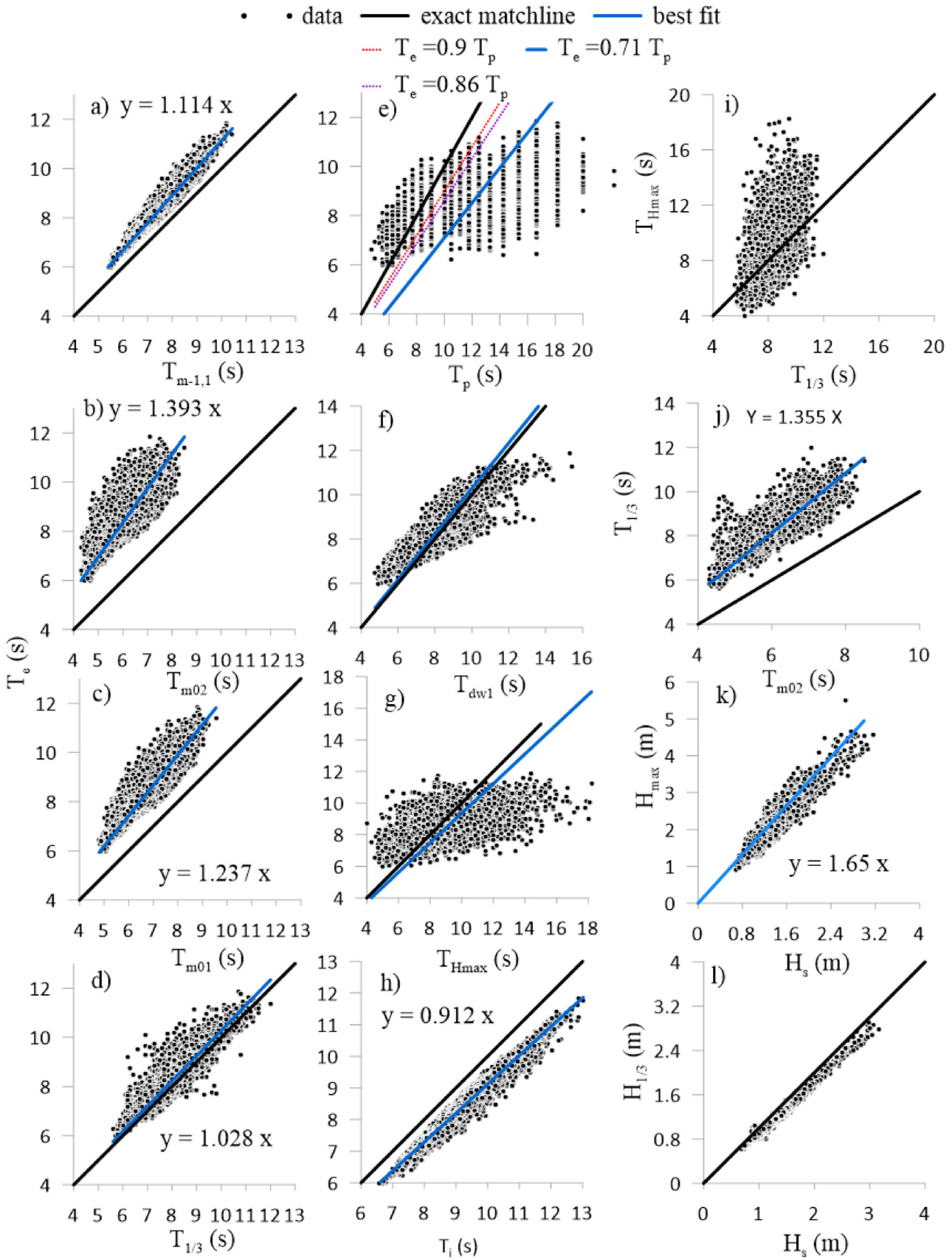

Fig. 4 Inter comparison of T_e with various wave periods for the 1 year wave data in 2015; **a** $T_{m-1,1,}$ **b** T_{m02}, **c** T_{m01}, **d** $T_{1/3}$, **e** T_p, **f** T_{dw1}, **g** T_{Hmax}, **h** $T_{i,}$. Scatter plots of **i** $T_{1/3}$ with T_{Hmax}, **j** T_{m02} with $T_{1/3}$, **k** H_s with H_{max}, and **l** H_s with $H_{1/3}$

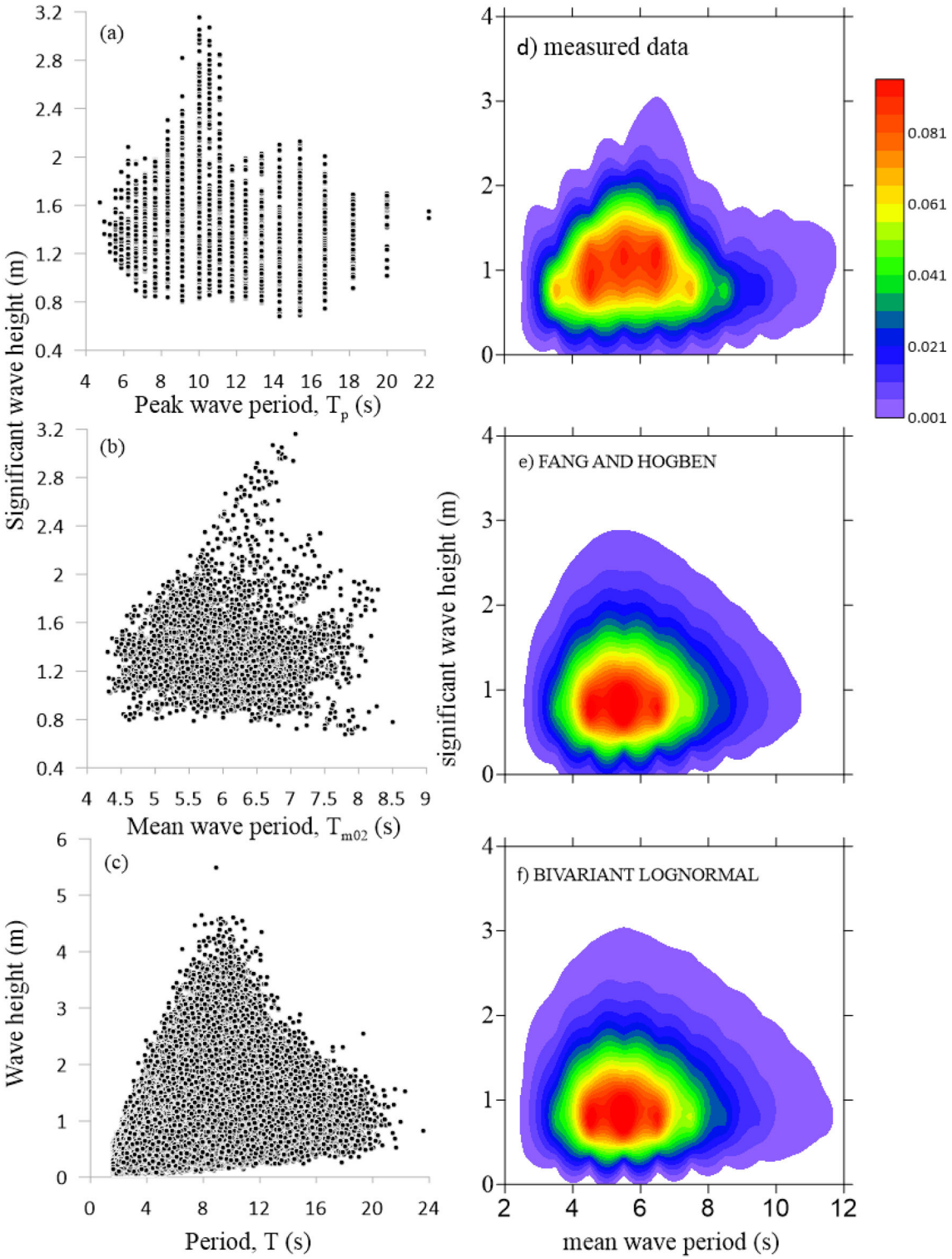

Fig. 5 Left panel shows the scatter plots of wave height and period. **a** Peak wave period and significant wave height, **b** mean wave period and significant wave height, **c** period and height of individual waves. Right panel is the contour plots showing the joint distribution of significant wave height and mean wave period during the year 2015 **d** measured data, **e** Fang and Hogben model, **f** Bivariate lognormal distribution

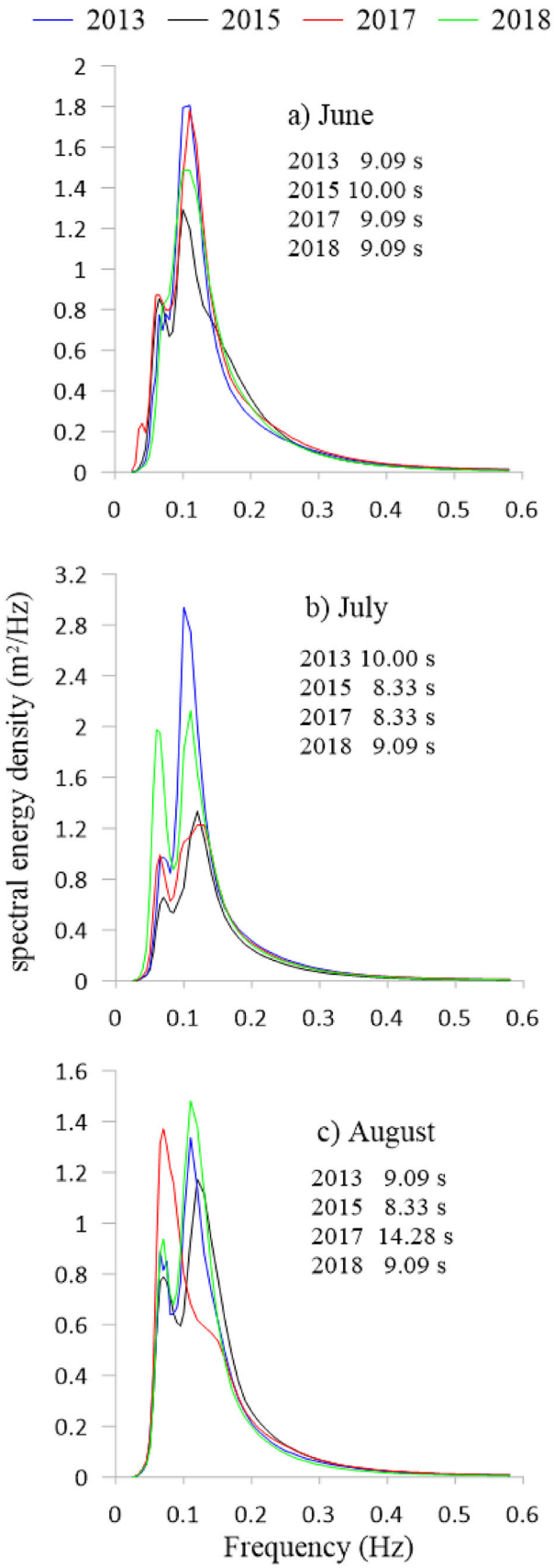

Fig. 6 Monthly average wave spectrum in different years. **a** June, **b** July and **c** August

3.3 Joint distribution of wave height and wave period

Once the significant wave height is determined using long-term distribution, there arises the problem of associating it with a mean wave period or peak period. The scatter plots of T_p with H_s indicate that waves with H_s more than 2.5 m are associated with T_p between 10 and 12 s (Fig. 5a). The waves with H_s more than 2 m have T_{m02} between 6 and 8 s (Fig. 5b). Similarly, waves with height more than 4 m are with period between 8 and 12 s (Fig. 5c). Joint distribution of H_s and T_{m02} shows that distribution of wave periods is broader than that of the wave heights, since the waves measured are mainly swells (Fig. 5d). Goda (2000) observed that distribution of wave periods is narrower than that of wave heights in wind seas. Both the models of the joint distribution of H_s and T_{m02} considered in the study indicate that the models are in good agreement with the overall trend of the measured data (Fig. 5e, f). Liu et al. (2020) also observed that bivariate lognormal distribution and the Fang and Hogben model are in good agreement with the measured wave data in the coastal waters of the South China Sea.

3.4 Interannual variations in the wave period

The distribution of different wave periods of individual waves from June to August for different years is analysed. The analysis shows that higher wave periods ($T_p > 8$ s) are greater for the year 2013 and lower period waves ($T_p < 6$ s) are more in 2015. The monthly average wave spectrum indicates that the wave spectra show two peaks (Fig. 6). Most of the spectral energy density of the sea surface height variance during June to August including both the spectral peaks are in the low-frequency bands corresponding to swells with T_p ranging from 8.33 to 14.28 s.

The 99-percentile values of T_{m02} are up to 15% (Fig. 7a). Mean values of T_{m02} for all the years of study are approximately the same (~ 6 s), while the 99-percentile values are high for the year 2013. In 2018, the mean value of T_c was 3.8 s, with the 99 and 90 percentile values reaching a maximum of 5.3 s and 4.6 s. The 99-percentile values are lower for the year 2015 except for T_c, T_{Hmax}, and T_p. A maximum seasonal mean value of 9.5, 9.3, and 8.9 s for T_{Hmax}, $T_{1/10}$, T_e is observed in the year 2017. The 90-percentile values of T_{m01} and $T_{1/3}$ are 8.5 and 10.6 s for 2017. Interannual variations in the mean values of T_{avg} (Fig. 7c) are less (< 5%).

3.5 Distribution of wavelength

For various years, the probability of exceedance of wavelength corresponding to different wave periods is estimated

and presented in Fig. 8 at Gopalpur and the statistical parameters are presented in Table 1. Mean values of λ_{Tp} and λ_{Tm02} are 123.7 and 56.7 m with a minimum-to-maximum value of 29.4 to 263.9 m for λ_{Tp} (Fig. 8a) and 25.4 to 112.6 m for λ_{Tm02} (Fig. 8b). The wavelength based on the period of the highest wave ranged from 23.7 to 231.4 m (Fig. 8 h). The percentage occurrence plots of wavelength based on wave period during monsoon and non-monsoon months are presented in Fig. 3c, d. The standard deviation values of λ_{Ti} and λ_{Tm01} are 17.1 and 14.3 m, respectively, and when compared with other parameters, λ_{Tp} exhibits a large standard deviation. For waves with $T_{\mathrm{p}} > 5$ s, the wavelength based on peak wave period (λ_{Tp}) varies from 42.2 to 263.9 m. Wavelength based on crest period (λ_{Tc}) ranges between 9.4 and 53 m with a mode value of 19 m (Fig. 8e). The values of the wavelength corresponding to λ_{Tdw2} and λ_{Tdw1} go up to a maximum of 155.6 m (Fig. 8f) and 277.6 m (Fig. 8g) and a minimum value of 39 m and 30.5 m, while the standard deviation of λ_{Tdw1}, $\lambda_{TH\mathrm{max}}$ is ~ 29 m. A maximum occurrence of 18.91% (Fig. 3c) is observed in between 85 and 90 m during monsoon months and about 1.67% (Fig. 3d) is observed for λ_{Tp} for the same interval during non-monsoon months. During non-monsoon months, for higher wavelength (150–155 m), the occurrence of λ_{Tp} is higher (15.90%) compared to that during the monsoon (5%). The values for λ_{Tc} vary up to 53 m and show a peak in occurrence percentage for values between 10 and 20 m (Fig. 3c, d). The wavelength based on the average wave period ($\lambda_{T\mathrm{avg}}$) and significant wave period ($\lambda_{T1/3}$) shows a mean value of 61 and 90.4 m for the study period. Interannual variation in the 90-percentile of the average wavelength is up to 9.84%. Wavelength based on significant wave period ($T_{1/3}$) is less than 90 m during 51% of the time. The occurrence of $\lambda_{\mathrm{T1/10}}$ is maximum in between 80 and 85 m with a percentage of 16.3 during monsoon and 4.14% during non-monsoon months. Around 17.2% is seen for λ_{Te} in between 95 and 100 m during monsoon months. Variations are seen in the occurrence percentage of wavelength associated with different wave periods during monsoon and non-monsoon months.

3.6 Interannual variations in the wavelength corresponding to various wave periods

The interannual variations of wavelength based on different wave periods for four different years are shown in Fig. 7d–f. Figure 7d shows a decrease in 99-percentile values for the year 2015 except for $\lambda_{TH\mathrm{max}}$, λ_{Tp}, and λ_{Tc}. Most of the time, higher values for 90-percentiles are observed during 2017 for various parameters. The wavelength based on average wave period ($\lambda_{T\mathrm{avg}}$) is mostly concentrated in a range between 28.8 and 135.3 m and the 90-percentile and mean values show an interannual variation of up to 10% and 7% (Fig. 7e, f). The 99-percentile values of $\lambda_{T\mathrm{avg}}$ are around 104.8 m for the year 2013. Interannual variations in the 90-percentile value of λ_{Tp} are up to 9% (Fig. 7e).

The 90-percentile and the mean value of λ_{Tm02} are 76 and 59.4 m, and the 90-percentile and mean values are higher for the years 2013 and 2018. For all the years, the values of λ_{Tc} are concentrated in the range of 9.4 to 53 m. A maximum 99-percentile value of 226, 172.4, 157.2, and 165.1 m is observed for λ_{Tdw1}, $\lambda_{T1/10}$, $\lambda_{T1/3}$, and λ_{Ti}. The mean values of λ_{Tm01} are 71.5 m and higher in 2018 and $\lambda_{TH\mathrm{max}}$ are 101.7 m with higher values in 2017. The values of λ_{Te} vary between 46.9 and 174.6 m with a maximum mean value of 94.5 m in 2017 and the 90-percentile value (106.7 m) is lower for 2015. Interannual variations in mean values of λ_{Te} are only up to 7% (Fig. 7f).

3.7 Monthly variations in wave period and its corresponding wavelength during 2015

Monthly variations of wave period and its corresponding wavelength are presented in Fig. 9 for the year 2015. Earlier in this study, interannual variation and the distribution of all parameters during the monsoon months (June, July, and August) for different wave periods and the corresponding wavelength are analysed. In this section, the analysis of average, 99-percentile, and 90-percentile of different parameters throughout a year is studied. Figure 9 shows a rise in various wave periods and the corresponding wavelength except for the parameters T_{p} and λ_{Tp} during October, November, and December, which might be caused by the influence of northeast monsoons or swells, or distant storms.

Strong winds from the southwest provide longer period waves during the southwest monsoon, whereas winds from the northeast cause shorter period waves during the northeast monsoon. The analysis has shown that the values of $T_{\mathrm{p}} > 8$ s during the northeast monsoon season are 91%. During the northeast monsoon period, even though short-period waves are present, the results show the presence of more long-period waves which might be caused due to the presence of swells and distant storms during this period. About 51% of values of wavelength corresponding to T_{p} are more than 100 m during the monsoon months and 87% of the values are higher than 100 m during non-monsoon months. The 99-percentile values of T_{c} and λ_{Tc} range from 4 to 5.4 s and 39 to 44 m for various months. The average values for 2015 for the parameters T_{m02}, T_{m01}, T_i, and $T_{H\mathrm{max}}$ are 6, 6.9, 9.2, and 8.7 s. The 90-percentile values of $\lambda_{T\mathrm{p}}$, λ_{Tdw1}, $\lambda_{T\mathrm{avg}}$, and λ_{Te} are 194.8, 106, 85, and 122.4 m.

3.8 Distributions of wave steepness and wavelength

The distribution of wave steepness and wavelength at Gopalpur for different years during the monsoon months of June, July, and August is presented in Fig. 10. The wave

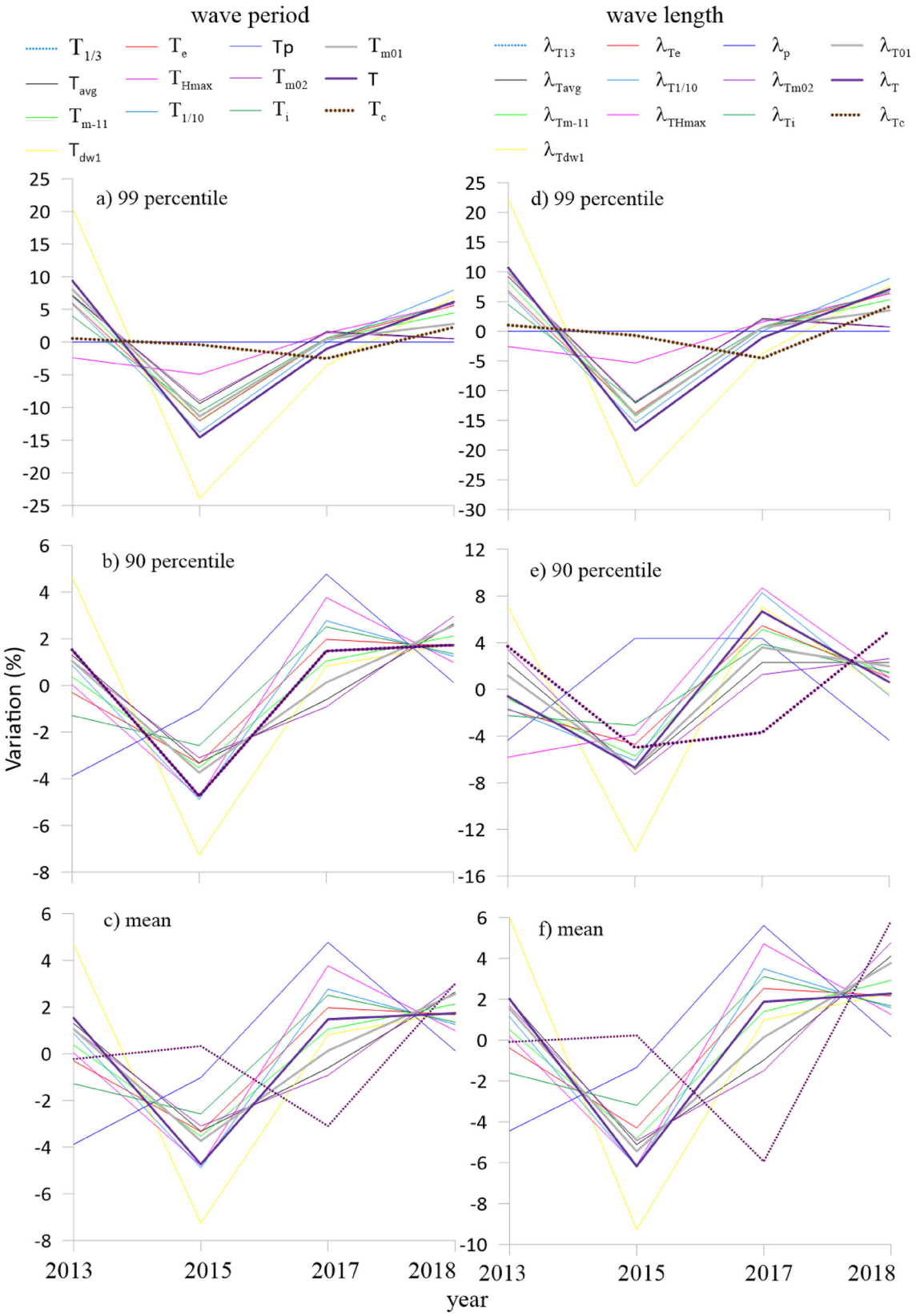

Fig. 7 Interannual variations in 99-percentile, 90-percentile and mean values of different wave periods (**a**–**c**) and corresponding variations in wavelength (**d**–**f**) in June to August 2013, 2015, 2017 and 2018

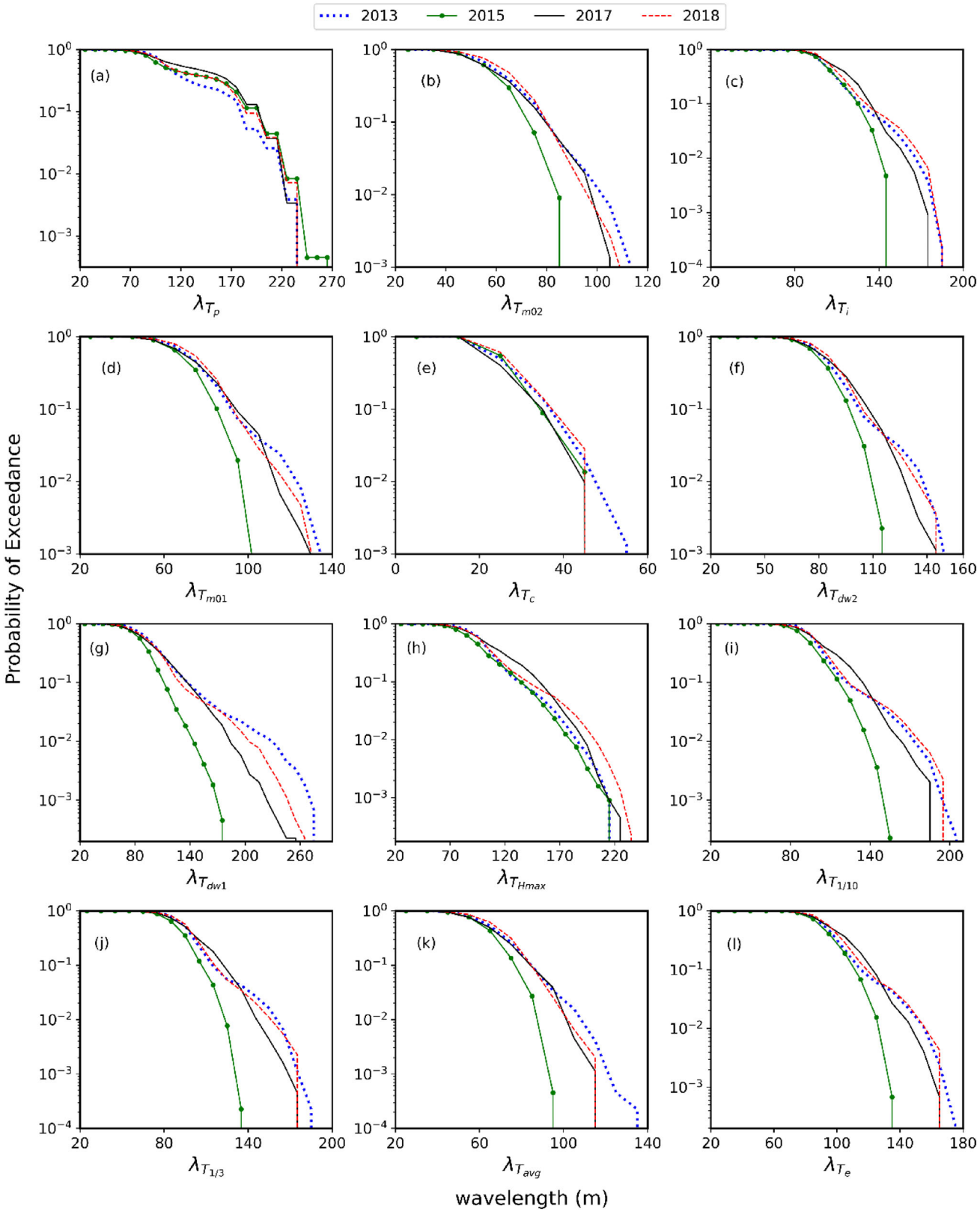

Fig. 8 Distribution of various wavelength corresponding to different wave periods for 4 years during the monsoon months June–August

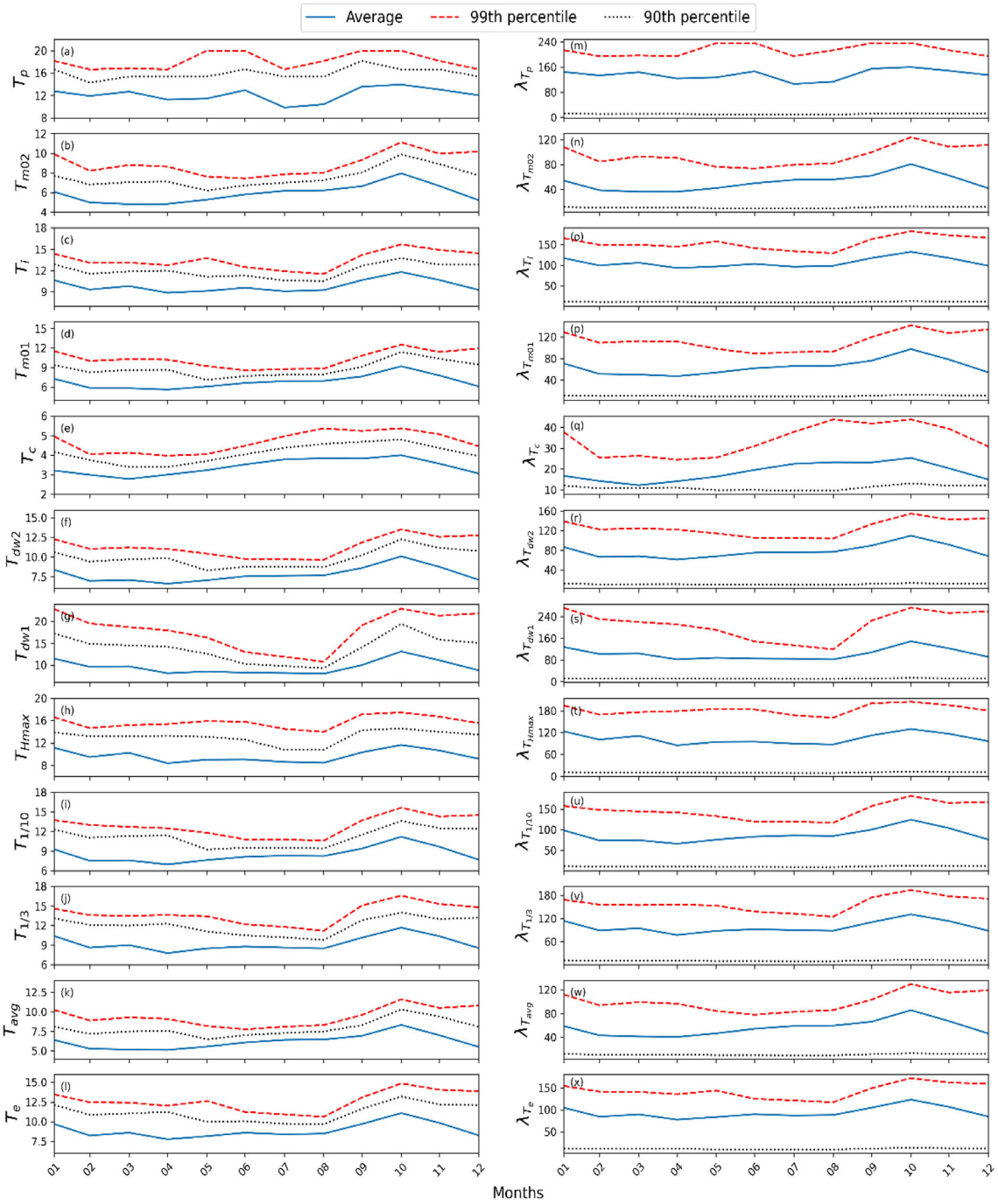

Fig. 9 Monthly variation of various wave period and its corresponding wavelength during 2015

steepness at the study region varied from 0.0002 to a maximum value of 0.2170 and for minimum steepness values, the wavelength ranges from 79 to 178 m. An average steepness value of ~ 0.018 is noticed during the entire year. A few waves with a period less than 1.7 s, height less than 1 m, and wavelength ranging between 4 and 4.5 m, exceed the wave-breaking limit. The most common values of wave period (T) range from 4 to 6.5 s. The shift in monsoon intensity causes significant variations in the temporal distribution of wave steepness over the eastern Arabian Sea, and the coastal waters along the central west coast of India are similar in terms of changes in wave steepness over a distance of around 325 km, but the southeastern Arabian Sea exhibits significant differences (Anju and Kumar 2023).

At Gopalpur, the values of the wavelength range from 4 to 283 m with the highest value of wavelength in 2017. For

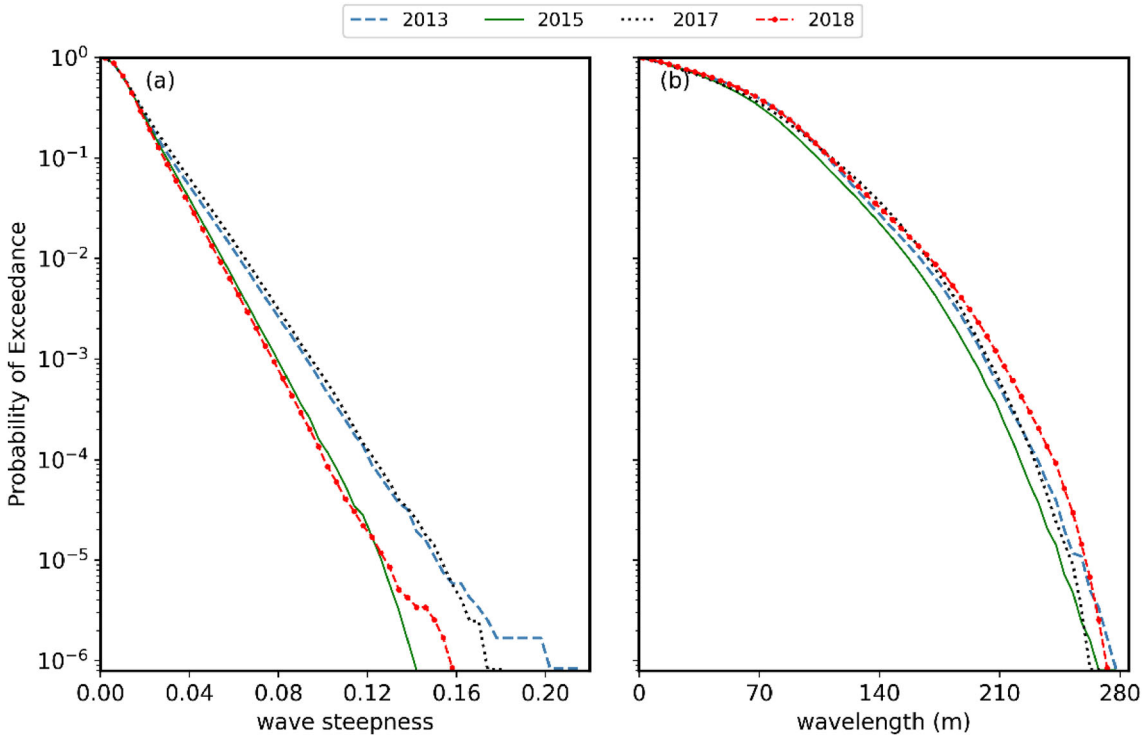

Fig. 10 Distribution of **a** wave steepness and **b** wavelength for different years during monsoon months June, July, and August

waves with wavelength < 5 m, the steepness values exceed the wave-breaking limit (0.1428 tanh kd). Higher values of wavelength ranging between 272 and 283 m are observed and its corresponding wave steepness varies from 0.002 to 0.006. Most of the time waves with higher steepness values have wavelengths ranging between 4 and 7 m. The maximum wavelength varies between 94 and 99 m for waves with a height of more than 5 m and their wave period is ~ 9 s for different years.

3.9 Variations in wave power

In 2015, H_s varied from 0.3 to 3.3 m with higher waves during the SW monsoon (June–August) and during the cyclone (Fig. 11a). The peak wave period ranged from 2.9 to 22 s with an annual mean value of 12.2 s (Fig. 11b). 50% of the time, T_p is between 10 and 14.3 s. The mean wave direction of 50% of the data is from 152 to 163° (Fig. 11b). For the study location, large fetch (> 1600 km) is available in the directional sector from 150° to 190° and hence, long period waves reach the measurement location from this directional sector. Since the nearshore bathymetry and the coastline have an inclination of ~ 48°to the east, the waves after refraction will approach the coast close to 138°. At the measurement location, the wave power ranges up to 45 kW/m in the monsoon period, while the annual mean wave power is 5 kW/m (Fig. 11d). 50% of the time, the wave power is between 2 and 7 kW/m, and 25% of the time, the wave power is more than 7 kW/m.

3.9.1 Analysis of selected freak wave events

This section analyses the freak wave events in Gopalpur in 2015. Freak waves with $H_{1/3}$ greater than 1.5 m are only considered since freak waves with low wave heights do not pose problems to marine operations. Out of 17,519 data, it is observed that as per H_{max}/H_s criteria around 37 freak wave events occurred and 11 events occurred as per the second criteria. Among this, by applying all the conditions, there are 5 freak wave events, and the characteristics of waves during these freak wave events are listed in Table 2. For the freak wave events, the values $H_{1/3}$ vary from 1.5 to 2.1 m, steepness varies between 0.035 and 0.052 and the wavelength varies between 76.1 and 98.2 m. Among the freak waves that occurred, the highest $H_{1/3}$ (2.1 m) and H_{max} (4.5 m) are in June.

According to Shrira and Slunyaev (2014), opposing currents trap surface gravity waves and the nonlinear dynamics associated with these waves significantly increase the probability of generating freak waves. The crest to significant wave height ratio is more for freak wave event 3. The freak wave event numbered 4 (Table 2) has a high abnormality index of about 2.22 and the steepness is higher for the freak wave event 3 (Table 2). There are three events of freak waves with

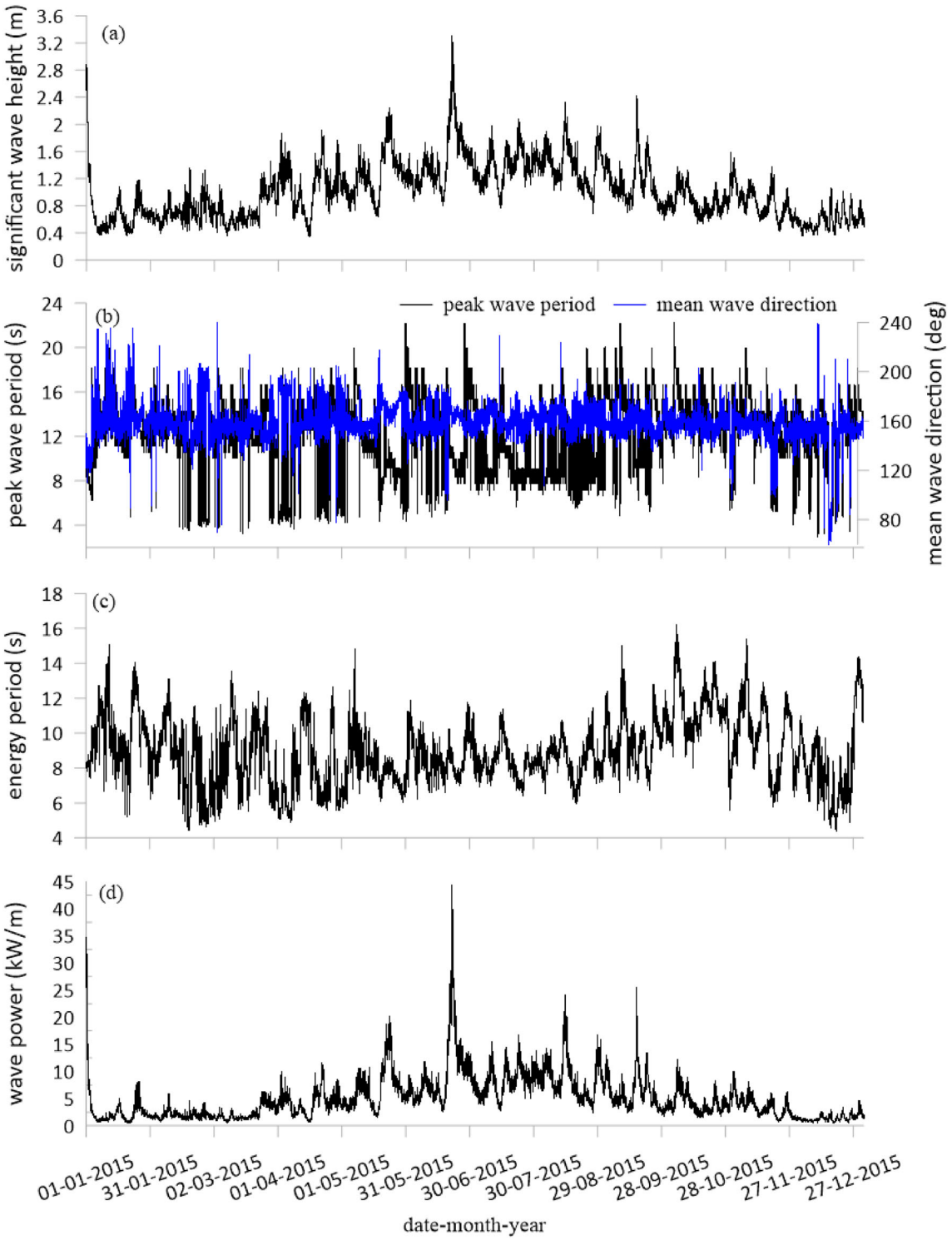

Fig. 11 Time series plots of **a** significant wave height, **b** peak wave period and mean wave direction, **c** energy period and **d** wave power for the year 2015

Table 2 Characteristics of selected freak waves occurred during 2015

Freak wave events	Date	Time (hhmm)	H_{max} (m)	$H_{1/3}$ (m)	$H_{max}/H_{1/3}$	T_p (s)	$H_{c\,(m)}$	$H_c/H_{1/3}$	Wavelength (m)	Steepness
1	22-05-2015	2147	3.7	1.7	2.18	8.5	2.2	1.27	88.7	0.042
2	22-06-2015	1734	4.5	2.1	2.13	9.2	2.8	1.32	98.2	0.046
3	22-06-2015	2004	4.1	2.0	2.04	7.8	2.7	1.38	77.5	0.052
4	29-08-2015	1904	3.4	1.5	2.22	9.1	1.9	1.26	96.9	0.035
5	30-08-2015	0634	3.4	1.6	2.06	7.6	2.1	1.29	76.1	0.044

values of T_p greater than 8 s with the H_s values being 1.7, 2.1, and 1.5 m, which indicates that the major amount of energy is contributed by long-period swells and the other two events have T_p between 6 and 8 s, and the energy is contributed by intermediate period waves. On analysing freak wave events, the values of T_p vary between 7.6 and 9.2 s so the presence of intermediate and long-period waves is not significant.

4 Discussion

In practice, when the wave parameters are obtained from a numerical model, $T_{1/3}$ and T_{Hmax} are not available in the absence of time series data. Hence, it is necessary to know the relationship of T_{Hmax} and $T_{1/3}$ with T_{m02}. Coastal Engineering Manual (2008) and Goda (2000) relate T_{Hmax} is equivalent to $T_{1/3}$ and is equal to 1.1 to 1.3 times T_{m02}. For the study area, the best fit slope is 1.36 which is slightly outside the range of 1.1–1.3. James and Panchang (2022) reported that for waves off the UK coast, $T_{1/3}$ is 1.43 times T_{m02}. For the study area, T_{Hmax} is not equivalent to $T_{1/3}$ and there is a large scatter for T_{Hmax} compared to values of $T_{1/3}$. At Gopalpur, the annual average T_{mo2} for all the years is up to 6.2 s and the annual average T_p is about 11.2 s. According to Mendes and Oliveira (2021), the average T_{m02} values at Faro, Nazare, and Leixoes fall within the range of 6–7 s, varying from a minimum of 3 s to a maximum of 15 s. Remya et al. (2020) reported a general decrease in mean wave period across most of the Indian Ocean suggesting that, while swells dominate the Indian Ocean, wind seas are becoming more important during June–August if a positive IOD, La Nina, and a positive phase of SAM co-occur or develop independently. Zhou et al. (2020) observed a weak correlation (0.47) between T_p and T_{mean}, and the T_p-to-T_{mean} ratio was determined to be 2.04 and $T_{1/3}$ and T_{m02} displayed a significant linear correlation with T_{mean}, while T_{max} and T_p exhibited a less pronounced linear correlation with T_{mean}.

The average wave steepness value for Gopalpur in the present study is about 0.018. Glejin et al. (2013) observed that the steepness is greater than 0.25 for an ocean dominated by wind sea. In the Indian Ocean, the steepness ranges between 0.01 and 0.25 when the sea is dominated by young swell (Majumder et al. 2022). In the deep waters of the Norwegian continental shelf, the average wave steepness for wind-sea falls within the 0.031–0.046 range, while for combined swell and wind-sea, the values span a broader range of 0.0054–0.125 (Myrhaug 2018). Mendes and Oliveira (2021) reported an approximate average value of steepness as 0.031 in the deep waters off the coast of Portugal. The steepness of the highest waves varied from 0.048 to 0.082, with the highest value observed at the northern location and the lowest at the southern location in the Arabian Sea (Anju and Kumar 2023).

A total of five freak wave events out of 37 events were analysed in the present study in the year 2015. In the South China Sea, between May and August, the probability of occurrence of observed freak waves falls within the range of 0.03–0.53% (Ji et al. 2022). Over a 6-year period, wave measurements taken at 11 locations in the southern North Sea reveal that the frequencies of freak waves remain consistently uniform across seasons and show no correlation between stations (Teutsch et al. 2020).

5 Conclusion

The variations in the wave steepness, wave period, and wavelength of ocean surface waves in the coastal waters, which are crucial for assessing hazards, ensuring safe navigation, designing coastal infrastructure, and studying beach dynamics are examined. The various wave periods measured at 15 m water depth are analysed and their corresponding wavelength is also presented. The values of the peak wave period (T_p) indicate that most of the time a swell dominance is seen at the coastal waters of Gopalpur. The percentage of $T_p > 8$ s is about 86%, whereas only 1% of waves are with periods less than 6 s in the monsoon. The energy wave period (T_e) plays an important role in describing wave energy and $T_e >$ 12 s is more in 2018. Half of the record shows that waves with wavelengths based on crest period (λ_{Tc}) are less than 21 m. The analysis of the relationship of T_e with various wave periods shows that T_e is in good relation with $T_{m-1,1}$,

$T_{1/3}$, and T_i. Wavelength based on significant wave period ($\lambda_{T1/3)}$ is less than 90 m during 51% of the time at Gopalpur. The values of λ_{Tp} exhibit a large standard deviation. The interannual variation of mean values of λ_{Tavg} is about 7%. The variations in the mean values of T_{avg} are up to 5%. During 2015, due to the presence of swells and distant storms large presence of long-period waves are observed. Analysis of the monthly variations for 2015, shows an increase in different parameters during the post-monsoon period. Among the five freak wave events, freak waves with higher maximum wave height (H_{max}) and significant wave height ($H_{1/3}$) are observed in June. In three freak wave events, the values of T_p are higher than 8 s, and the values for five events vary between 7.6 and 9.2 s. A higher abnormality index is noted for freak wave event 4, with a value of 2.22. The results have practical implications, aiding in the selection of a suitable wave energy converter for the study location and the analysis of freak waves provides information regarding abnormal wave characteristics. Comprehending the variations in wave characteristics on monthly, annual, and interannual scales is vital for a range of applications, including coastal engineering and navigation.

Acknowledgements The author gratefully acknowledges the financial support given by the Council of Scientific and Industrial Research, New Delhi to conduct this research. The measured wave data used in the study are from the project funded by the Earth System Science Organization, Ministry of Earth Sciences, Government of India through INCOIS, Hyderabad. We thank both the reviewers and the editor for their critical comments and suggestions which improved the scientific content of this paper. This is NIO contribution ---.

Author contributions Anju T M: Conceptualization, Formal analysis, Data curation, Writing –original draft Sanil Kumar V: Conceptualization, Supervision, Writing – review & editing. Rabindro Nath Samal: Data curation All authors reviewed the manuscript.

Data availability The measured data used in this article is available for joint research work from the corresponding author.

Declarations

Competing interests The authors declare no competing interests.

References

Amrutha MM, Kumar VS (2017) Characteristics of high monsoon wind-waves observed at multiple stations in the eastern Arabian Sea. Ocean Sci Discuss. https://doi.org/10.5194/os-2017-84

Amrutha MM, Kumar VS (2022) Evaluation of a few wave energy converters for the Indian Shelf seas based on available wave power. Ocean Eng 244:110360. https://doi.org/10.1016/j.oceaneng.2021.110360

Amrutha MM, Sanil Kumar V, Anoop TR, Balakrishnan Nair TM, Nherakkol A, Jeyakumar C (2014) Waves off Gopalpur, northern Bay of Bengal during Cyclone Phailin. Ann Geophys 32:1073–1083. https://doi.org/10.5194/angeo-32-1073-2014

Anjali Nair M, Kumar VS, Amrutha MM (2018) Spectral wave characteristics in the nearshore waters of northwestern Bay of Bengal. Pure Appl Geophys 175:3111–3136. https://doi.org/10.1007/s00024-018-1838-5

Anju TM, Kumar VS (2023) Steepness of surface gravity waves measured in the eastern Arabian Sea during peak monsoon months. Ocean Eng 280:114900. https://doi.org/10.1016/j.oceaneng.2023.114900

Balaguru K, Taraphdar S, Leung LR, Foltz GR (2014) Increase in the intensity of post monsoon Bay of Bengal tropical cyclones. Geophys Res Lett 41(10):3594–3601. https://doi.org/10.1002/2014GL060197

Bitner-Gregersen EM, Guedes Soares C, Silvestre A (1998) On the average wave steepness. In: Proc. Ocean Wave Kinematics. Dynamics and Loads on Ship Structures (Wave'98). ASCE, Houston, USA, pp. 513–520

Bromirski PD, Cayan DR, Flick RE (2005) Wave spectral energy variability in the northeast Pacific. J Geophys Res 110:C03005. https://doi.org/10.1029/2004JC002398

Chen W, van der Werf JJ, Hulscher SJMH (2023) A review of practical models of sand transport in the swash zone. Earth Sci Rev 238:104355. https://doi.org/10.1016/j.earscirev.2023.104355

Chun H, Ahn K (2017) Storm waves on the East coast of Korea: 20 years of wave hindcasting. J Coast Res 33(5):1182–1188. https://doi.org/10.2112/JCOASTRES-D-16-00139.1

Coastal Engineering Manual (2008) U.S. Army Corps of Engineers.

Contestabile P, Ferrante V, Vicinanza D (2015) Wave energy resource along the coast of Santa Catarina (Brazil). Energies 8(12):14219–14243. https://doi.org/10.3390/en81212423

Datawell (2009) Datawell Waverider reference manual. Datawell BV Oceanographic Instruments, p 123

Fang ZS, Hogben N (1982) Analysis and prediction of long term probability distributions of wave heights and periods. National Maritime Institute, Report R146, London.

George J, Kumar VS (2021) Spectral peak wave period climatology and its relationship with natural climate variability over the Bay of Bengal. Ocean Dyn 71:871–892. https://doi.org/10.1007/s10236-021-01473-w

Glejin J, Kumar VS, Nair TMB (2013) Monsoon and cyclone induced wave climate over the near shore waters off Puduchery, south western Bay of Bengal. Ocean Eng 72:277–286. https://doi.org/10.1016/j.oceaneng.2013.07.013

Glejin J, Kumar VS, Nair TMB, Singh J, Nherakkol A (2014) Freak waves off Ratnagiri, west coast of India. Indian J Geo-Mar Sci 43(7):1339–1342

Goda Y (2000) Random seas and design of maritime structures. Advanced Series on Ocean Engineering, vol 33. World Scientific Inc., Singapore

Gramstad O, Bitner-Gregersen E, Trulsen K, Borge JCN (2018) Modulational instability and rogue waves in crossing sea states. J Phys Oceanogr 48(6):1317–1331. https://doi.org/10.1175/JPO-D-18-0006.1

Haver S (2001) Evidences of the existence of freak waves. In: Rogue waves. Ifremer Brest, pp 129–140

Hofland B, Chen X, Altomare C, Oosterlo P (2017) Prediction formula for the spectral wave period Tm-1,0 on mildly sloping shallow foreshores. Coast Eng 123:21–28. https://doi.org/10.1016/j.coastaleng.2017.02.005

James JP, Panchang V (2022) Investigation of wave height distributions and characteristic wave periods in coastal environments. J Geophys Res Oceans 127:e2021JC018144. https://doi.org/10.1029/2021jc018144

Ji X, Li A, Li J, Lei W, Daoru W (2022) Research on the statistical characteristic of freak waves based on observed wave data. Ocean Eng 243:110323. https://doi.org/10.1016/j.oceaneng.2021.110323

Kraus NC, Larson M (1988) Beach Profile Change Measured in the Tank for Large Waves 1956–1957 and 1962. Technical Report CERC-88–6.

Kumar VS, Dubhashi KK, Balakrishnan Nair TM (2014) Spectral wave characteristics off Gangavaram, Bay of Bengal. J Oceanography 70(3):307–321. https://doi.org/10.1007/s10872-014-0223-y

Kumar VS, George J, Joseph D (2020) Hourly maximum individual wave height in the Indian shelf seas—its spatial and temporal variations in recent 40 years. Ocean Dyn 70:1283–1302. https://doi.org/10.1007/s10236-020-01395-z

Lavrenov IV (1998) The wave energy concentration at the Agulhas current off South Africa. Nat Hazards 17:117–127. https://doi.org/10.1023/A:1007978326982

Liu XL, Cai ZW, Sun Z, Chen WW, Jun Y, Ding J, Ye YL (2020) Study on long-term distribution and short-term characteristics of the waves near islands and reefs in the SCS based on observation. Ocean Eng 218:108171. https://doi.org/10.1016/j.oceaneng.2020.108171

Longuet-Higgins MS (1983) On the joint distribution of wave periods and amplitudes in a random wave field. Proc R Soc Lond A Math Phy Sci 389(1797):241–258. https://doi.org/10.1098/rspa.1983.0107

Majumder S, Remya PG, Nair TB, Sirisha P (2022) Analysis of meteorological and oceanic conditions during freak wave events in the Indian Ocean. Ocean Eng 259:111920. https://doi.org/10.1016/j.oceaneng.2022.111920

Mendes D, Oliveira TCA (2021) Deep-water spectral wave steepness offshore mainland Portugal. Ocean Eng 236:109548. https://doi.org/10.1016/j.oceaneng.2021

Muller P, Garrett C, Osborne A (2005) Rogue waves. Oceanography 18:66

Myrhaug D (2018) Some probabilistic properties of deep-water wave steepness. Oceanologia 60:187–192. https://doi.org/10.1016/j.oceano.2017.10.003

Ochi MK (1978) On long-term statistics for ocean and coastal waves. Coast Eng Proc 2:59–75. https://doi.org/10.1061/9780872621909.004

Patra A, Bhaskaran PK (2017) Temporal variability in wind–wave climate and its validation with ESSO-NIOT wave atlas for the head Bay of Bengal. Clim Dyn 49:1271–1288. https://doi.org/10.1007/s00382-016-3385-z

Patra SK, Mishra P, Mohanty PK, Pradhan UK, Panda US, Ramana Murthy MV, Nair TMB (2016) Cyclone and monsoonal wave characteristics of northwestern Bay of Bengal: long-term observations and modeling. Nat Hazards 82:1051–1073. https://doi.org/10.1007/s11069-016-2233-0

Perlin M, Choi W, Tian Z (2013) Breaking waves in deep and intermediate waters. Annu Rev Fluid Mech 45:115–145. https://doi.org/10.1146/annurev-fluid011212-140721

Remya PG, Kumar BP, Srinivas G, Nair TMB (2020) Impact of tropical and extra tropical climate variability on Indian Ocean surface waves. Clim Dyn 54:4919–4933. https://doi.org/10.1007/s00382-020-05262-x

Shrira VI, Slunyaev AV (2014) Nonlinear dynamics of trapped waves on jet currents and rogue waves. Phys Rev E 89(4):041002. https://doi.org/10.1103/PhysRevE.89.041002

Stansell P, Wolfram J, Linfoot B (2004) Improved joint probability distribution for ocean wave heights and periods. J Fluid Mech 503:273–297. https://doi.org/10.1017/S002211200400802X

Stokes GG (1880) Considerations relative to the greatest height of oscillatory irrotational waves which can be propagated without change of form. On the theory of oscillatory waves. Cambridge University Press, London, pp 225–229

Teutsch I, Weisse R, Moeller J, Krueger O (2020) A statistical analysis of rogue waves in the southern North Sea. Nat Hazards Earth Syst Sci 20:2665–2680. https://doi.org/10.5194/nhess-20-2665-2020

Tucker MJ (1991) Waves in ocean engineering: measurement, analysis, interpretation. Ellis Horwood, Chichester, p 431

Zhao M, Deng X, Wang J (2022) Description of the joint probability of significant wave height and mean wave period. J Mar Sci Eng 10:12. https://doi.org/10.3390/jmse10121971

Zhou Y, Ye Q, Shi W, Yang B, Song Z, Yan D (2020) Wave characteristics in the nearshore waters of Sanmen Bay. Appl Ocean Res 101:102236. https://doi.org/10.1016/j.apor.2020.102236